Vanda Oliveira*, Jan Van den Bulcke, Joris Van Acker, Thomas de Schryver and Helena Pereira

Cork structural discontinuities studied with X-ray microtomography

Abstract: Cork is a natural cellular material with a rather unique set of properties, and its best known application is as stopper for wine bottles. The cork tissue contains structural discontinuities, for example, lenticular channels (LCh), that influence the in-use performance of cork products. X-ray microtomography, in combination with image analysis, has been used for cork characterisation and provided new insights into the three-dimensional location of discontinuities, which are hidden for a visual inspection. It was demonstrated that the presence of LCh is positively correlated with cork density, and the void fraction of LCh in the lower part of a cork stopper is strongly related to the oxygen ingress in the bottle during the first month after bottling. The results contribute to better understanding the natural variation of cork properties.

Keywords: cork, image processing, lenticular channels, natural cork stoppers, structural discontinuities, X-ray microtomography

DOI 10.1515/hf-2014-0245
Received September 9, 2014; accepted December 12, 2014; previously published online xx

Introduction

Cork is produced from the bark of *Quercus suber* L. Its properties as a lightweight material are unique. For example, it is viscoelastic and allows large deformation under compression without fracture, largely impermeable to water and other liquids and gases, a thermal and electric insulator, and an acoustic and vibration absorber (Fortes et al. 2004; Pereira 2007). Cork is best known as a successful bottle closure since ancient times (Pereira 2007) and is still the most popular closure, especially for long-term aging of red wines (Phillips 2014).

The cork tissue has a honeycomb structure with a considerable regularity in the cellular arrangement: the cells are closed and noncommunicating, with thin walls that surround an air-filled lumen; the cell volume is, on average, 1.7×10^{-5} mm^3, and its solid content is around 13.5%. However, the tissue contains discontinuities that influence the in-use performance of cork products and are thereby closely associated with the commercial value of raw cork and of cork products (Pereira 2007). Lenticular channels (LChs) are the most important features in this context: they cross the cork layers from the outside to the inner tissue and are loosely filled with a dark brown, unsuberified material, usually conspicuous to visual observation (Pereira et al. 1996; Oliveira et al. 2012). Other discontinuities can have an accidental occurrence, such as the galleries made by the larva of *Coroebus undatus* or by the ant *Crematogaster scutellaris* (Gonzalez-Adrados and Pereira 1996; Pereira 2007).

X-ray imaging in its two-dimensional (2D) form is widely used in wood science for microdensitometry studies (Ikonen et al. 2008; Boden et al. 2010; Helama et al. 2012; Knapic et al. 2014). X-ray tomography is a nondestructive 3D imaging technique that allows the study of interior structures of an object (Landis and Keane 2010). Industrial X-ray tomography scanners are successful for determination of wood properties in terms of internal log features such as pith, growth rings, heartwood and sapwood, knots, and decay (Wei et al. 2011; Longuetaud et al. 2012).

X-ray microtomography (XRMT) has a higher spatial resolution and has been proved to be of value in different fields such as biomedicine (Kim et al. 2014), geoscience (Cnudde and Boone 2013), and material science (Dewanckele et al. 2012; Česen et al. 2013). In wood science, 3D XRMT was employed to study the shrinkage behaviour of cells (Taylor et al. 2013), the analysis of coatings (Van den Bulcke et al. 2010; Bessières et al. 2013), the compressive

***Corresponding author: Vanda Oliveira,** Universidade de Lisboa, Instituto Superior de Agronomia, Centro de Estudos Florestais (CEF), Tapada da Ajuda, P-1349-017 Lisboa, Portugal,
e-mail: vandaoliveira@isa.ulisboa.pt.
http://orcid.org/0000-0003-3461-7028
Jan Van den Bulcke and Joris Van Acker: UGCT-Woodlab-UGent, Faculty of Bioscience Engineering, Department of Forest and Water Management, Ghent University, Coupure Links 653, 9000 Ghent, Belgium
Thomas de Schryver: UGCT, Centre for X-ray Tomography, Department of Physics and Astronomy, University Ghent, Proeftuinstraat 86, 9000 Ghent, Belgium
Helena Pereira: Universidade de Lisboa, Instituto Superior de Agronomia, Centro de Estudos Florestais (CEF), Tapada da Ajuda, P-1349-017 Lisboa, Portugal. http://orcid.org/0000-0002-5393-4443

behaviour of low-density fibreboard (Tran et al. 2013), wood anatomical details (Van den Bulcke et al. 2009), the pore structure of paper (Axelsson and Svensson 2010), wood composites (Wieland et al. 2013), and dendrochronology (Van den Bulcke et al. 2013).

XRMT was not yet applied for cork characterisation, which is usually performed by image analysis of the surface, in the course of which the internal discontinuities remain concealed (Pereira et al. 1996). Brunetti et al. (2002) applied Compton tomography in the study of cork stopper density to refine the visual classification. Hor et al. (2008) evaluated and imaged natural cork by means of terahertz spectroscopy. Donepudi et al. (2010) visualised images of cork stoppers with a novel imaging technology, called diffraction-enhanced imaging.

The present work explores XRMT for the visualisation and quantification of cork structural discontinuities. These discontinuities are decisive for the commercial value of raw cork and of cork products as they are a possible pathway for air, impregnation liquids and microbial penetration. The expectation is that XRMT may contribute to a better understanding of the natural variation in cork (Oliveira et al. 2013) and that it can contribute to the development of an improved monitoring of its key features in terms of an increased quality of existing cork products as well as to the design of new products.

Materials and methods

Ten natural cork stoppers (24 mm diameter×45 mm length) were selected, produced in one major Portuguese cork producer before washing and surface treatment. The stoppers were punched out from cork planks and classified in three visual quality classes (premium, good, and standard). Their surface (lateral and top surface) was imaged with photographic equipment and subsequently processed by image analysis according to the procedure of Oliveira et al. (2012). The objects that can be visualised with adequate thresholding (in general, called cork pores) can be individually characterised quantitatively. The porosity coefficient (%), defined as the proportion of the area occupied by pores, was calculated (Oliveira et al. 2012).

Then, bottles were closed by the stoppers and oxygen ingress measurements were performed using a nondestructive colorimetric method, by which oxidation was detected by means of an indigo carmine solution (Oliveira et al. 2013). The total amount of oxygen that had reached the interior of the bottle 30 days after closure was taken as a key feature, as it is an indicator for the quick and high oxygen ingress in the first days after bottling.

An XRMT instrument built at the Centre for X-ray Computed Tomography (UGCT, Ghent University, Belgium; www.ugct.ugent.be) was applied. The scanner used at Woodlab-UGent, further referred to as Nanowood, is specifically designed to obtain very high resolution scans as well as scans of larger objects. The instrument is equipped with a generic in-house developed computed tomography scanner control software platform (Dierick et al. 2010) that allows full control of the scanner hardware (see Dierick et al. 2014). For all stoppers, a total of 900 projections were acquired over an angle of 360°. All stoppers were reconstructed using Octopus 8.6, a server/client tomography reconstruction package for parallel and cone beam geometry (Vlassenbroeck et al. 2007), resulting in a voxel size of 50 μm for a scan covering the entire stopper.

Image processing and analysis were performed using the Fiji image processing package (Schindelin et al. 2012) and Morpho+ (Vlassenbroeck et al. 2007; Brabant et al. 2011), aiming at noise removal, image enhancement, and feature extraction. Morpho+ was used in combination with a bilateral filter (nonlinear, edge-preserving, and noise-reducing smoothing filter) to perform histogram equalisation for contrast improvement.

A circular region of interest was manually selected within each stack, which is representative for the transverse (Tv) cork stopper section. Segmentation was performed by means of an automated thresholding based on the isodata algorithm (Ridler and Calvard 1978). A single threshold level was selected for pores and another one for high-density regions (HDRs) through the entire volume. When focusing on the void fraction, every data point was assigned to either background (solid material) or foreground (voids), and the closing mathematical morphology operator was applied to the binary images to fill misclassified pixels inside the pores as well as to maintain pore connections.

The void volume was calculated using the "3D Object Counter" plugin (Bolte and Cordelières 2006). The 3D void fraction coefficient was calculated by dividing the total volume of voids by the volume of interest. The same analysis was done for the 3D characterisation of HDR.

Data analysis was performed using Microsoft Excel 2010. The results from the analysis of the X-ray volumes were compared with data from previous measurements of surface image analysis, density, and oxygen ingress. All statistical correlation and regression analyses were performed by means of the SPSS statistical software (version 22.0; SPSS Inc., Chicago, IL).

Results and discussion

Visual observation of cork structural discontinuities

Different materials can be distinguished by XRMT based on their differences in X-ray absorption coefficient at each point and due to the relationship of these data to material density. The 3D internal structure of cork can also be inferred, which is typically displayed as a series of 2D "slices," and LChs can be visualised in different sections. Figure 1A illustrates different sections in the three orthogonal planes, i.e., in tangential (Tg), radial (R), and Tv directions. The anisotropy of LCh is clearly observable, which is closely related to their biological development within the corkboard and the orientation

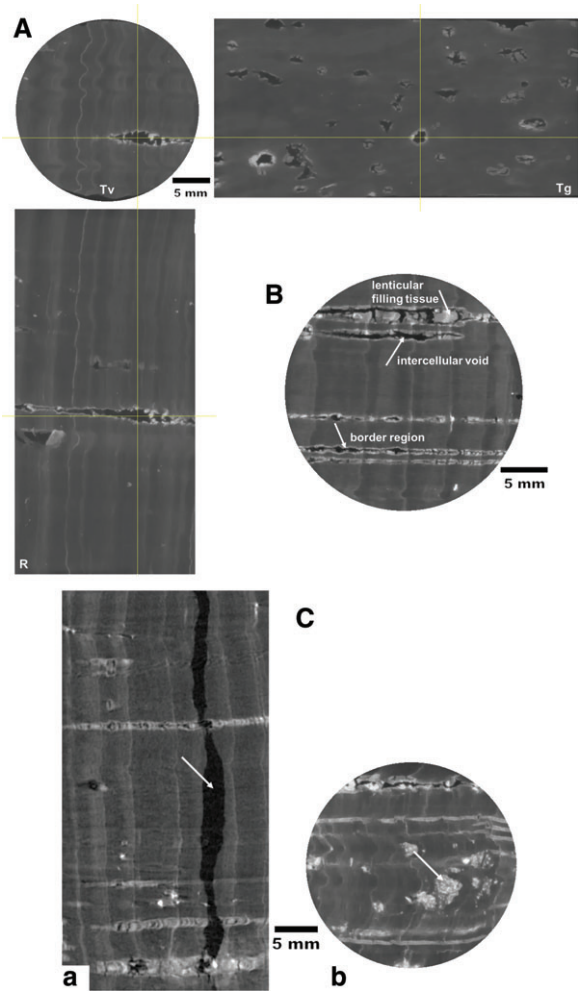

Figure 1 (A) Typical 2D "slices" from a 3D greyscale image of a cork stopper scanned at 50 μm resolution.
Different sections through the cork stopper in three orthogonal planes: Tv, R, and Tg. Crossing lines represent the same point in the three images. (B) Tv greyscale image with identification of lenticular filling tissue, intracellular voids and the border region of the LChs. And (C) Defects in the cork structure: (a) empty ant gallery and (b) "nail" lignocellulosic inclusion.

of the cutting process during stopper production (Pereira 2007). LChs have a tubular form, and in Tv and R planes, they appear as linear strands. In each slice, only parts of the channels are observed (Figure 1A) because the Tv plane does not coincide with the LCh development axis. However, the full development of the LCh can be well observed in the orthogonal R plane, while in the Tg slices, the LChs are sectioned perpendicularly to their axis and look rounded. These observations can be compared with the surface seen by image analysis of the main sections of cork planks (Pereira et al. 1996; Gonzalez-Adrados et al. 2000) and of cork stoppers (Oliveira et al. 2012).

The observed geometry of the LCh certainly impacts the cork properties for applications where bending properties are of importance (Anjos et al. 2011a). Figure 1B corroborates that LChs are loosely filled with a tissue of rigid unsuberified cells with thick walls, showing ruptures and intercellular voids in a great extent (Pereira 2007). It is also visible that the region bordering the LCh has higher density than the surrounding material does due to the presence of lignified and thick-walled cells at their borders (Figure 1B).

Additionally, cork may also contain features of biological or external origin that are classified as defects in practical application. Such features could also be observed by XRMT. As mentioned in the Introduction, *C. undatus* F. larvae and several species of ants that excavate galleries that run through the cork plank may be the origin of such defects. The larvae galleries are filled with residual material, while the ant galleries are usually empty and have a random direction. They can appear at the cork stopper surface only as a small hole, which may go unnoticed even to expert operators but cause wine leakage. Figure 1Ca shows the development from top-to-top of one of these empty ant galleries in a premium classified cork stopper.

Another possible defect is the inclusion of small portions of lignified cells within the cork tissue, referred to in the cork jargon as "nail". These cells have thick walls and a lignocellulosic chemical composition, and therefore, their density is well above the density of the surrounding cork tissue (Pereira 2007). Figure 1Cb shows these nail inclusions as HDRs. The above-mentioned defects can be scanned with an approximate voxel pitch of maximally 0.1 mm.

Quantitative analysis and 3D characterisation

Table 1 summarises the main features of the stoppers in focus. The stoppers (St) were selected to cover a wide range of properties: the lateral surface porosity coefficient ranged from 1.1% (St 2 and 4) to 8.6% (St 7); top surface porosity coefficient ranged from 0.7% (St 1) to 4.7% (St 7); density ranged from 152.0 kg m^{-3} (St 8) to 262.7 kg m^{-3} (St 7); total amount of oxygen ingress at 30 days ranged from 1.4 mg (Sts 1 and 7) to 4.0 mg (St 9).

Figure 2 illustrates the structure of internal cork discontinuities. By thresholding the voids and HDRs, the internal LCh network becomes observable. Figure 2a shows the surface of the cork St comparable to what image analysis could reveal by photography. Figure 2b shows the void fraction consisting mainly of intracellular voids, and

Table 1 Characterization of the natural cork stoppers: lateral and top surface porosity coefficient, density, and oxygen ingress at 30 days after bottling.

Stopper	Visual class	Porosity coeff. (lateral) (%)	Porosity coeff. (top) (%)	Density (kg m^{-3})	Oxygen ingress at 30 days (mg)
1	Premium	1.8	0.7	182.8	1.4
2	Premium	1.1	1.3	166.9	3.6
3	Premium	1.4	1.3	185.5	3.5
4	Premium	1.1	1.3	161.9	1.6
5	Good	3.9	3.1	227.8	2.5
6	Good	2.2	3.4	205.4	3.4
7	Standard	8.6	4.7	262.7	1.4
8	Standard	6.3	1.7	152.0	3.3
9	Standard	4.5	1.3	224.8	4.0
10	Standard	3.4	4.0	196.8	2.6

Figure 2c shows the void fraction (green) and the HDRs (red). It is noticeable that these HDRs preferably appear bordering the void fraction.

The quantification of 3D structural discontinuities is summarised in Table 2. For each St the following are presented: the void and HDR volume; the void fraction and the HDR fraction, defined as the proportion of the volume occupied by the void or HDR regions; the maximum void or HDR volume, defined as the largest single connected structure; and the porosity coefficient, calculated as the sum of the void and the HDR fractions. This XRMT porosity coefficient was calculated to establish the relation with image analysis measurements. In fact, image analysis of the cork St surface distinguishes the LCh by adequate thresholding but does not discriminate between voids and HDRs.

The void fraction ranged from 0.7% (St 4) to 2.3% (St 9), while the maximum single void volume ranged from 7.9 mm^3 (St 6) to 104.9 mm^3 (St 9). The total HDR volume ranged from 231 mm^3 (St 4) to 2747 mm^3 (St 7), corresponding to a HDR fraction of 1.3% and 19.2%, respectively. The high HDR volume of St 7 corresponds to a single connected structure measuring 2468 mm^3. The cork St 3 that was classified as a premium St (i.e., low porosity coefficient by image analysis and high visual quality) had one of the highest total void volume (404 mm^3).

Relating surface image analysis and XRMT

Quality classes of natural cork Sts depend on the apparent homogeneity of their external surface, as seen by human eye or machine vision (Fortes et al. 2004; Pereira 2007). The heterogeneity of the cork surface is given by the presence of LCh, woody inclusions, small fractures, or other defects that can be identified by image analysis and are referred to as the porosity of cork (Gonzalez-Adrados and Pereira 1996; Pereira et al. 1996). Figure 3a shows the correlation between the lateral surface porosity coefficient calculated by image analysis (Oliveira et al. 2012) and the interior porosity coefficient calculated using XRMT.

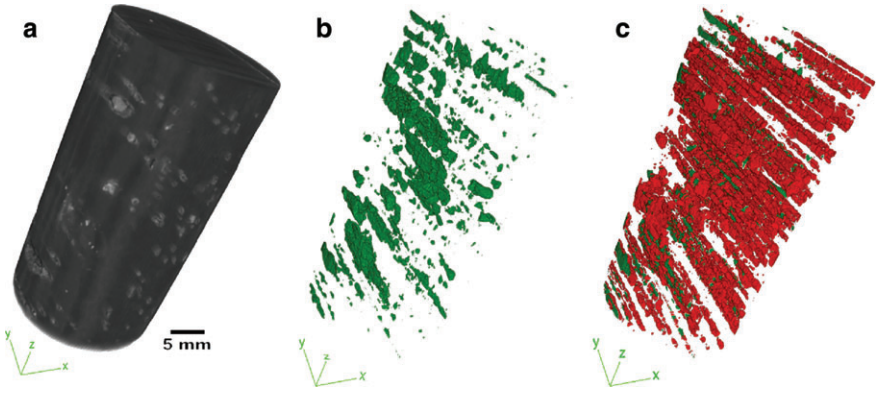

Figure 2 3D overview: (a) rendered volume of a cork stopper, (b) the void fraction of cork stopper structural discontinuities, and (c) cork stopper structural discontinuities colour coded: in red, the high density regions; and in green, the void fraction.

Table 2 Characterisation of 3D structural discontinuities of natural cork stoppers: voids and HDRs.

Stopper	Void volume (mm^3)	Void fraction (%)	Maximal void (mm^3)	HDR volume (mm^3)	HDR fraction (%)	Maximal HDR (mm^3)	Porosity coeff. (%)
1	159.9	0.9	62.6	512.9	3.0	208.8	3.9
2	176.8	0.8	22.1	328.1	1.6	39.0	2.4
3	403.8	1.8	86.9	829.6	3.7	48.6	5.5
4	127.4	0.7	21.2	231.0	1.3	20.3	2.0
5	217.7	1.1	23.5	1247.1	6.1	480.9	7.2
6	163.6	1.0	7.9	853.2	5.0	221.1	5.9
7	184.4	1.3	17.4	2747.0	19.2	2467.8	20.5
8	399.3	1.9	64.7	609.7	2.9	292.4	4.8
9	486.1	2.3	104.9	2406.7	11.5	1065.2	13.8
10	329.9	2.0	52.0	90.7	0.6	6.4	2.6

Because these two variables quantify porosity (LCh and other defects), a linear fit was used for data evaluation. Pearson's correlation analysis shows a positive linear relationship between the two data sets (r=0.78, R^2=0.61, and R_{aj}=0.56) (P<0.008). St 7 significantly influences this linear fit, which is an example for a high-porosity material due to woody inclusions. Nevertheless, the variability between the samples is evident in Figure 3a. For instance,

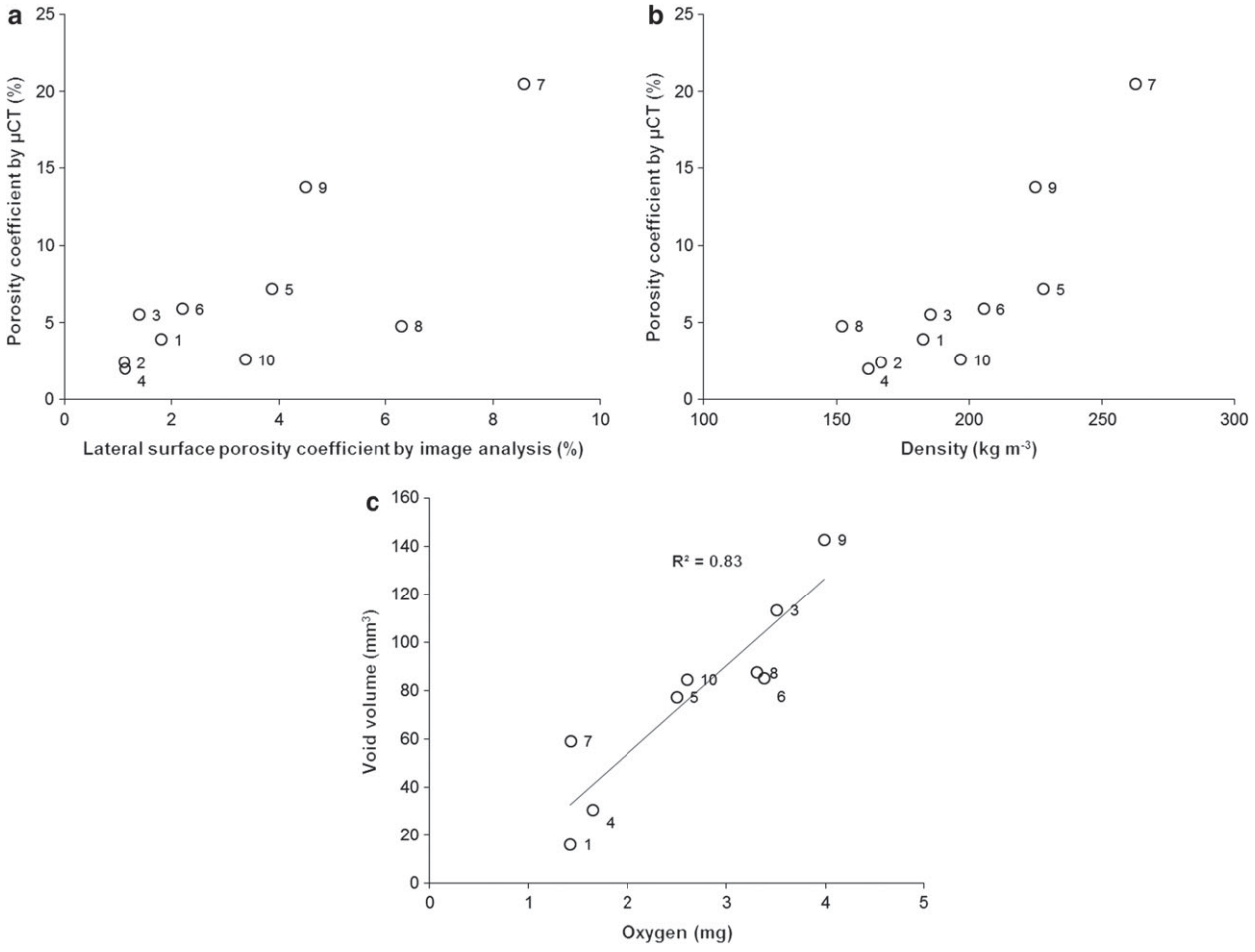

Figure 3 (a) Relation between the porosity coefficient calculated by image analysis and XRMT; (b) Relation between air-dried cork density and the porosity coefficient calculated by XRMT; and (c) Relation between the void volume in the bottom third part of the cork stopper and the oxygen ingress 30 days after bottling.

Sts 8 and 10, both classified as standard and with lateral surface porosity coefficient of 6.3% and 3.4%, respectively, have a smaller porosity coefficient calculated with XRMT (4.8% and 2.6% respectively), meaning that the interior of these cork Sts has less discontinuities than predicted by visual analysis of the surface. On the other hand, Sts 7 and 9, also classified as standard with lateral surface porosity coefficient of 8.6% and 4.5%, have 20.3% and 13.8% porosity coefficient calculated with XRMT due to the presence of nail regions. Accordingly, surface imaging and XRMT may give deviating results concerning LCh. Moreover, when considering the porosity coefficient calculated for the Tv section (top) by image analysis, the Pearson's correlation (r) is only 0.47 (R^2=0.22 and R_{aj}=0.12) (P<0.173).

Calculating the porosity coefficient by XRMT for all Tv slices of each St separately (to assess internal heterogeneity) resulted in an averaged coefficient of variation of 74%. This very high value corroborates the existence of an important axial variation in the tree (coincident with the St axis) and, therefore, a probable occurrence of large between-top differences in a St since they correspond to two different axial positions in the tree. Oliveira et al. (2012) obtained a median value of 2.1 for a porosity ratio calculated between tops, with extreme between-top differences (15.3% and 0.2% in the two tops of the same St).

This indicates that the Tv porosity coefficient that serves for quality grading of cork Sts, and which is derived from the cutting of the cork planks into parallel strips, does not give reliable information about the internal structure of LCh.

Density and porosity relationship

The density of air-dried cork tissue is low (150–160 kg m^{-3}), but there are also extremes around 120 to over 200 kg m^{-3} (Pereira 2007). In the first instance, it is conceivable that the numerous voids could reduce the density of cork, but this is not the case, and a relation between density and the void fraction was not found. This means that porosity in cork is not equivalent to voids. The reason is that the LChs are filled with nonsuberous material and, in some cases, delineated by thick-walled lignified cells (Anjos et al. 2008).

Against the expectation, the extent of LCh is positively related to cork density, with an r of 0.85 (R^2=0.72 and R_{aj}=0.69) (P<0.0001), as seen in Figure 3b. González-Hernández et al. (2014) also applied a linear fit to relate porosity and density and found a moderate positive correlation (r=0.58, P<0.0001). The higher r value in the present study can be related to the sample size and the presence of Sts 7 and 9 that have a high porosity and density due to the presence of woody inclusions. Anjos et al. (2014) reported that porosity increased from the lower to the higher density class of cork Sts and presented scanning electron microscope (SEM) cork images showing the concentration of sclerenchymatic cells in the region surrounding the LCh.

The lignocellulosic inclusions (nail) observed in cork Sts 5, 7, and 9 increase the density of cork to values above 200 kg m^{-3}. Nail inclusions influence fracture propagation under tensile stress (Anjos et al. 2011b).

Oxygen ingress and porosity relationship

The contact between wine and oxygen is of critical importance for wine conservation and the in-bottle aging process (Godden et al. 2005), and thus, the oxygen ingress through cork Sts was also investigated. Despite the large variability between cork Sts, there is a common logarithmic behaviour of oxygen ingress as a function of time (Oliveira et al. 2013). There is quick and high oxygen ingress in the first days after bottling, with an initial high ingress rate, followed by a decreasing ingress rate until the first month, and further on stabilizing at a low and rather constant ingress rate from the 3rd to the 12th month. Ribéreau-Gayon (1933) suggested that the initial high oxygen ingress is due to the high internal pressure in the cork cells created when the cork Sts are compressed into the bottleneck (see also Lopes et al. 2007). Therefore the initial high ingress rate of oxygen into the bottle should be related to the cork structural discontinuities, i.e., more specifically to the void fraction and the air located there. Apart of the first period, gas transport through the cork cells occurs with very low diffusion rates through small channels (i.e., through the plasmodesmata) present in the cork cells walls (Faria et al. 2011).

The void volume in the lower part of the St was calculated by taking only the 1/3 of the St, i.e., the part in contact to the bottled liquid. The relationship between the void volume of this 1/3 St and the amount of oxygen diffused during 30 days after bottling is presented in Figure 3c.

The linear regression established between these data has a coefficient of determination (R^2) of 0.83 and adjusted R^2 of 0.81. These results suggest that the high oxygen ingress rates immediately after bottling are due to the transfer of the air trapped in the voids in the bottom part of the cork St. This knowledge is relevant for the cork industry, which means that the orientation of the St must be carefully attended, i.e., the question which top of the St should be in contact with the wine.

Conclusions

XRMT was successfully applied for visualisation and quantification of cork structural discontinuities, which are decisive for the commercial value of raw cork and of cork products. The results demonstrated that image analysis of cork stoppers surface as used for quality grading has a poor relation with the internal structure quantification. The presence of LChs is positively correlated with cork density. The void fraction of LCh in the innermost part of the cork stopper inserted in the bottle is strongly related to the oxygen ingress in the first month after bottling. The results can be interpreted that XRMT scanning as quality control for stopper production may improve essentially the quality control. In view of the availability of rapid XRMT scanning set-ups, this kind of approach seems to be feasible.

Acknowledgments: Financial support by the Transnational Access to Research Infrastructures activity in the 7th Framework Programme of the EC under the Trees4Future project (no. 284181) for conducting the research is gratefully acknowledged. This work was partially supported by FEDER funds through the Operational Programme for Competitiveness Factors – COMPETE – and by National Funds under the project FCOMP-01-0124-FEDER-005421.

The research was carried out under the framework of Centro de Estudos Florestais, a research unit funded by Fundação para a Ciência e Tecnologia, Portugal (PEst OE/AGR/UI0239/2014). Funding from FCT is acknowledged by the first author as a doctoral student (SFRH/BD/77550/2011). The authors acknowledge the collaboration of Amorim & Irmãos, S. A. in materials supply.

References

Anjos, O., Pereira, H., Rosa, M.E. (2008) Effect of quality, porosity and density on the compression properties of cork. Holz Roh Werkst. 66:295–301.

Anjos, O., Pereira, H., Rosa, M.E. (2011a) Characterization of radial bending properties of cork. Eur. J. Wood Prod. 69:557–563.

Anjos, O., Pereira, H., Rosa, M.E. (2011b) Tensile properties of cork in axial stress and influence of porosity, density, quality and radial position in plank. Eur. J. Wood Prod. 69:85–91.

Anjos, O., Rodrigues, C., Morais, J., Pereira, H. (2014) Effect of density on the compression behaviour of cork. Mater. Des. 53:1089–1096.

Axelsson, M., Svensson, S. (2010) 3D pore structure characterization of paper. Pattern Anal. Appl. 13:159–172.

Bessières, J., Maurin, V., George, B., Molina, S., Masson, E., Merlin, A. (2013) Wood-coating layer studies by X-ray imaging. Wood Sci. Technol. 47:853–867.

Boden, S., Schinker, M.G., Duncker, P., Spiecker, H. (2010) Resolution abilities and measuring depth of high-frequency densitometry on wood samples. Measurement 45:1913–1921.

Bolte, S., Cordelières, F.P. (2006) A guided tour into subcellular colocalization analysis in light microscopy. J. Microsc. 224:213–232.

Brabant, L., Vlassenbroeck, J., De Witte, Y., Cnudde, V., Boone, M.N., Dewanckele, J., Van Hoorebeke, L. (2011) Three-dimensional analysis of high-resolution X-ray computed tomography data with Morpho+. Microsc. Microanal. 17:252–263.

Brunetti, A., Cesareo, R., Golosio, B., Luciano, P., Ruggero, A. (2002) Cork quality estimation by using Compton tomography. Nucl. Instrum. Methods Phys. Res., Sect. B 196:161–168.

Česen, A., Korat, L., Mauko, A., Legat, A. (2013) Microtomography in building materials. Mater. Technol. 47:661–664.

Cnudde, V., Boone, M.N. (2013) High-resolution X-ray computed tomography in geosciences: a review of the current technology and applications. Earth Sci. Rev. 123:1–17.

Dewanckele, J., De Kock, T., Boone, M.A., Cnudde, V., Brabant, L., Boone, M.N., Fronteau, G., Van Hoorebeke, L., Jacobs, P. (2012) 4D imaging and quantification of pore structure modifications inside natural building stones by means of high resolution X-ray CT. Sci. Total Environ. 416:436–448.

Dierick, M., Van Loo, D., Masschaele, B., Boone, M.N., Van Hoorebeke, L. (2010) A LabVIEW (R) based generic CT scanner control software platform. J. X-Ray Sci. Technol. 18:451–461.

Dierick, M., Van Loo, D., Masschaele, B., Van den Bulcke, J., Van Acker, J., Cnudde, L., Van Hoorebeke, L. (2014) Recent micro-CT scanner developments at UGCT. Nucl. Instrum. Methods Phys. Res. Sect. B 324:35–40.

Donepudi, V.R., Cesareo, R., Brunetti, A., Zhong, Z., Yuasa, T., Akatsuka, T., Takeda, T., Gigante, G.E. (2010) Cork embedded internal features and contrast mechanisms with DEI using 18, 20, 30, 36, and 40 keV synchrotron X-rays. Res. Nondestr. Eval. 21:171–183.

Faria, D.P., Fonseca, A.L., Pereira, H., Teodoro, O.M.N.D. (2011) Permeability of cork to gases. J. Agric. Food Chem. 59:3590–3597.

Fortes, M.A., Rosa, M.E., Pereira, H. A Cortiça. IST Press, Lisbon, 2004.

Godden, P., Lattey, K., Francis, L., Gishen, M., Cowey, G., Holdstock, M., Robinson, E., Waters, E., Skouroumounis, G., Sefton, M., Capone, D., Kwiatkowski, M., Field, J., Coulter, A., D'Costa, N., Bramley, B. (2005) Towards offering wine to the consumer in optimal condition – the wine, the closures and other packaging variables: a review of AWRI research examining the changes that occur in wine after bottling. Wine Ind. J. 20:20–30.

Gonzalez-Adrados, J., Pereira, H. (1996) Classification of defects in cork planks using image analysis. Wood Sci. Technol. 30:207–215.

Gonzalez-Adrados, J., Lopes, F., Pereira, H. (2000) Quality grading of cork planks with classification models based on defect characterisation. Holz Roh Werkst. 58:39–45.

González-Hernández, F., González-Adrados, J.R., Gracía de Ceca, J.L., Sánchez-González, M. (2014) Quality grading of cork stoppers based on porosity, density and elasticity. Eur. J. Wood Prod. 72:149–156.

Helama, S., Bégin, Y., Vartiainen, M., Peltola, H., Kolström, T., Meriläinen, J. (2012) Quantifications of dendrochronological information from contrasting microdensitometric measuring circumstances of experimental wood samples. Appl. Radiat. Isot. 70:1014–1023.

Hor, Y.L., Federici, J.F., Wample, R.L. (2008) Nondestructive evaluation of cork enclosures using terahertz/millimetre wave spectroscopy and imaging. Appl. Optics 47:72–78.

Ikonen, V.-P., Peltola, H., Wilhelmsson, L., Kilpeläinen, A., Väisänen, H., Nuutinen, T., Kellomäki, S. (2008) Modelling the distribution of wood properties along the stems of Scots pine (*Pinus sylvestris* L.) and Norway spruce (*Picea abies* (L.) Karst.) as affected by silvicultural management. For. Ecol. Manage. 256:1356–1371.

Kim, K., Yoon, H., Diez-Silva, M., Dao, M., Dasari, R., Park, Y. (2014) High-resolution three-dimensional imaging of red blood cells parasitized by *Plasmodium falciparum* and in situ hemozoin crystals using optical diffraction tomography. J. Biomed. Opt. 19: Article 011005.

Knapic, S., Pirralho, M., Louzada, J.L., Pereira, H. (2014) Early assessment of density features for 19 *Eucalyptus* species using X-ray microdensitometry in a perspective of potential biomass production. Wood Sci. Technol. 48:37–49.

Landis, E.N., Keane, D.T. (2010) X-ray microtomography. Mater. Charact. 61:1305–1316.

Longuetaud, F., Mothe, F., Kerautret, B., Krähenbühl, A., Hory, L., Leban, J.M., Debled-Rennesson, I. (2012) Automatic knot detection and measurements from X-ray CT images of wood: a review and validation of an improved algorithm on softwood samples. Comput. Electron. Agric. 85:77–89.

Lopes, P., Saucier, C., Teissedre, P.-L., Glories, Y. (2007) Main routes of oxygen ingress through different closures into wine bottles. J. Agric. Food Chem. 55:5167–5170.

Oliveira, V., Knapic, S., Pereira, H. (2012) Natural variability of surface porosity of wine cork stoppers of different commercial classes. J. Int. Sci. Vigne Vin 46:331–340.

Oliveira, V., Lopes, P., Cabral, M., Pereira, H. (2013) Kinetics of oxygen ingress into wine bottles closed with natural cork stoppers of different qualities. Am. J. Enol. Viticult. 64:3. doi:10.5344/ajev.2013.13009.

Pereira, H. Cork: Biology, Production and Uses. Elsevier, Amsterdam, 2007.

Pereira, H., Lopes, F., Graça, J. (1996) The evaluation of the quality of cork planks by image analysis. Holzforschung 50:111–115.

Phillips, C. (2014) Closure survey report: consistency key in selecting closures. Wine Business Monthly. XXI:18–28.

Ribéreau-Gayon, J. (1933) Dissolution d'oxygène dans les vins. In: Contribution à l'étude des oxidations et réductions dans les vins. Application à l'étude de vieillissement et des cases. Ed. Libraire Delmas. Bordeaux, France. pp. 35.

Ridler, T.W., Calvard, S. (1978) Picture thresholding using an iterative selection method. IEEE Trans. Syst. Man Cybern. SMC-8:630–632.

Schindelin, J., Arganda-Carreras, I., Frise, E., Kaynig, V., Longair, M., Pietzsch, T., Preibissch, S., Rueden, C., Saalfeld, S., Schmid, B., Tinevez, J.-Y., White, D.J., Hartenstein, V., Eliceiri, K., Tomancak, P., Cardona, A. (2012) Fiji: an open-source platform for biological-image analysis. Nat. Methods 9:676–682.

Taylor, A., Plank, B., Standfest, G., Petutschnigg, A. (2013) Beech wood shrinkage observed at the micro-scale by a time series of X-ray computed tomographs (μXCT). Holzforschung 67:201–205.

Tran, H., Doumalin, P., Delisee, C., Dupre, J.C., Malvestio, J., Germaneau, A. (2013) 3D mechanical analysis of low-density wood-based fiberboards by X-ray microcomputed tomography and digital volume correlation. J. Mater. Sci. 48:3198–3212.

Van den Bulcke, J., Boone, M., Van Acker, J., Stevens, M., Van Hoorebeke, L. (2009) X-ray tomography as a tool for detailed anatomical analysis. Ann. For. Sci. 66:508.

Van den Bulcke, J., Boone, M., Van Acker, J., Van Hoorebeke, L. (2010) High-resolution X-ray imaging and analysis of coatings on and in wood. J. Coat. Technol. Res. 7:271–277.

Van den Bulcke, J., Wernersson, E.L.G., Dierick, M., Van Loo, D., Masschaele, B., Brabant, L., Boone, M.N., Van Hoorebeke, L., Haneca, K., Brun, A., Hendriks, C.L.L., Van Acker, J. (2013) 3D tree-ring analysis using helical X-ray tomography. Dendrochronologia 32:39–46.

Vlassenbroeck, J., Dierick, M., Masschaele, B., Cnudde, V., Van Hoorebeke, L., Jacobs, P. (2007) Software tools for quantification of X-ray microtomography at the UGCT. Nucl. Instrum. Meth. Phys. Res. A 580:442–445.

Wei, Q., Leblon, B., La Rocque, A. (2011) On the use of X-ray computed tomography for determining wood properties: a review. Can. J. For. Res. 41:2120–2140.

Wieland, S., Grünewald, T., Ostrowski, S., Plank, B., Standfest, G., Mies, B., Petutschnigg, A. (2013) Assessment of mechanical properties of wood-leather panels and the differences in the panel structure by means of X-ray computed tomography. BioResources 8:818–832.